

Strong coupling phases of conserved growth models are crumpled

Debayan Jana^{1,*} and Abhik Basu^{1,†}

¹*Theory Division, Saha Institute of Nuclear Physics,
a CI of Homi Bhabha National Institute, 1/AF,
Bidhannagar, Calcutta 700064, West Bengal, India*

We show that stochastically driven nonequilibrium conserved growth models admit generic strong coupling phases for sufficiently strong nonlocal chemical potentials underlying the dynamics. The models exhibit generic roughening transitions between perturbatively accessible weak coupling phases satisfying an exact relation between the scaling exponents in all dimensions d , and strong coupling phases. In dimensions below the critical dimension d_c , the latter phases are unstable and argued to be crumpled, and thus distinct from the well-known strong coupling rough phase of the Kardar-Parisi-Zhang equation in dimensions $d \geq 2$. At d_c , conventional spatio-temporal scaling in the weak coupling phase is logarithmically modulated and are exactly obtained.

Strong coupling phases and roughening transitions in nonequilibrium systems have been an intense focus of research. The most famous example is the Kardar-Parisi-Zhang (KPZ) equation for surface growth without any conservation laws [1, 2], which undergoes a roughening transition from a smooth to a perturbatively inaccessible strong coupling rough surface at dimensions $d > 2$, as the noise strength or the nonlinear coupling strength is increased; see Ref. [3] for a comprehensive review on this subject. Perturbative inaccessibility of the strong coupling regime of the KPZ equation has promoted researchers to use extensive numerical methods [4–8] or mode coupling theories (MCT) [9–16] to extract the scaling behavior in the rough phase. Such roughening transitions to strong coupling phases have been observed in various generalizations of the KPZ equation, e.g., coupled KPZ [15, 16], KPZ with nonlocality [17, 18]. Subsequently, to account for conserved growth processes, conserved versions of the KPZ equation were proposed and studied. This includes the conserved KPZ (CKPZ) equation [19], which belongs to a distinct universality class without any roughening transition. A related model [20], (hereafter LDS equation) has the same form as the CKPZ equation, but driven by *nonconserved* noises [2, 20]. It was introduced to describe idealized MBE [2, 20, 21], particularly under high temperature conditions where surface diffusion of incoming atoms leads to smoother growth. The LDS equation belongs to a different universality class known as the LDS class that also lacks any roughening transition.

The CKPZ or LDS models were subsequently generalized to CKPZ+ model [22] and MBE+ model [23] respectively by considering nonlocal contributions to the underlying chemical potential μ . In the CKPZ+ model, there is a phase transition in dimensions $d > 1$, from the perturbatively accessible CKPZ universality class to a new, unstable, growth regime. Similarly, the MBE+ model [23] predicts a roughening transition for $d \leq 4$, between an algebraically rough phase (associated with the MBE class) and a strong coupling crumpled phase; and for $d > 4$, between a smooth phase (MBE class) and

a strong coupling algebraic rough phase.

In this Letter, we investigate the strong coupling phases and the associated roughening transitions in a general class of noisy conserved growth models with an underlying chemical potential μ controlling the dynamics containing a nonlocal part. We demonstrate that when the nonlocal component of μ is weak, the surfaces can be both linearly and nonlinearly stable, or linearly unstable. However, at stronger nonlocality the surfaces (including CKPZ+ and MBE+ equations in two dimensions (2D)) can become nonlinearly unstable, even if it is linearly stable, signaling a transition to strong coupling phases that are argued to be crumpled for $d \leq d_c$, the critical dimension of the model. Our results are obtained by a combination of perturbative calculations, nonperturbative reasoning, and numerical simulations.

We now proceed to derive these results, beginning with the equation of motion that governs the dynamics

$$\begin{aligned} \frac{\partial h}{\partial t} = & \bar{\nu} \nabla^2 h - \nu \nabla^4 h - \frac{\lambda}{2} \nabla^2 (\nabla h)^2 \\ & - \lambda_1 \nabla_i \nabla_j (\nabla_i h \nabla_j h) + \eta. \end{aligned} \quad (1)$$

In analogy with active membranes, we set $\nu > 0$ (analog of a bend modulus [24]), but similar to active tensions in active membranes, let $\bar{\nu}$ to be of any sign. Both λ, λ_1 are nonlinear coupling constants with arbitrary signs of the lowest order symmetry-permitted *active* terms. Noise η is zero-mean, Gaussian distributed with a variance

$$\langle \hat{\eta}(\mathbf{k}, t) \hat{\eta}(\mathbf{k}', t') \rangle = 2D |\mathbf{k}|^{-y} \delta^d(\mathbf{k} + \mathbf{k}') \delta(t - t'). \quad (2)$$

in the Fourier space, where \mathbf{k} is a wavevector. Here, $y \geq -2$ determines the spatial correlation of the noise. Eq. (1) implies a current \mathbf{J} and a chemical potential μ [22, 23] related via $\mathbf{J} = -\nabla \mu$, where

$$\begin{aligned} \mathbf{J} = & -\bar{\nu} \nabla h + \nu \nabla \nabla^2 h + \frac{\lambda}{2} \nabla [(\nabla h)^2] \\ & + \lambda_1 \nabla^{-2} \nabla [\nabla_i \nabla_j (\nabla_i h \nabla_j h)]. \end{aligned} \quad (3)$$

The λ_1 -term contributes nonlocally to μ [19, 20]. If $\bar{\nu} \geq (<)0$, the model is linearly stable (unstable) in the long wavelength limit; $\nu = 0$ is akin to a (mean-field)

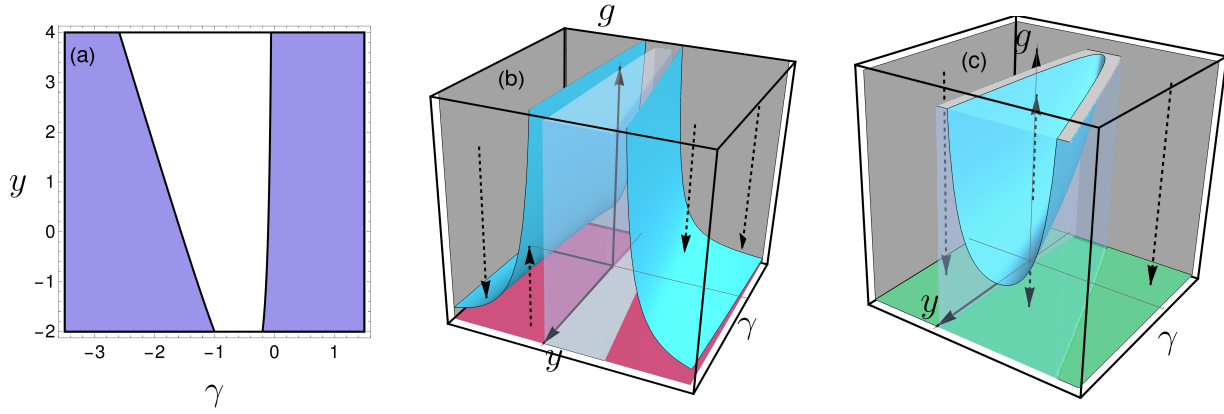


FIG. 1. ($\bar{\nu} = 0$) (a) Stable (violet) and unstable (white) regions in the γ - y plane as obtained from RG and MCT calculations at $d = d_c = 4 + y$. (b) RG flow diagram at $d < d_c$. The blue planes represent stable fixed planes toward which the RG flow lines (black dashed arrows) converge. The red region denotes the stable phase accessible via perturbation theory, while the central white region is speculated to be unstable. (c) RG flow diagram for $d > d_c$. The central white region contains a blue plane representing an unstable fixed plane, where a roughening transition occurs between a smooth phase (green region) and a perturbatively inaccessible strong coupling rough phase, as indicated by the RG flow lines. Outside this region, the roughening transition disappears, and only the smooth phase remains.

critical point in equilibrium critical systems. One can define a "correlation length" $\bar{\xi} \equiv \sqrt{\nu/|\bar{\nu}|}$, such that for a surface of linear size $L < (>)\bar{\xi}$, the long wavelength properties are controlled by $\nu(\bar{\nu})$. Focusing on the linearly stable case, we note that the correlation function $C(\mathbf{k}, \omega) \equiv \langle |h(\mathbf{k}, \omega)|^2 \rangle = 2Dk^{-y}/[\omega^2 + (\bar{\nu}k^2 + \nu k^4)^2]$ in the linear theory. It now behooves us to find whether non-linear effects are relevant (in the RG or renormalization group sense). We apply the perturbative Wilsonian dynamic renormalization group (RG) approach at one-loop order [2, 25, 26]. At the largest scales, where relaxation is dominated by the $\bar{\nu} > 0$ -term in (1), there are *no* relevant fluctuation-corrections to $\bar{\nu} > 0$ and D , giving the above result for C exact in the asymptotic long wavelength limit. For sufficiently small $\bar{\nu}$, there should be a large enough range of scales in which the dominant relaxation is controlled by the ν -term. Once again we apply RG, which we remind the reader is only valid on length scales $L < \bar{\xi}$. This is implemented via a path integral formalism in terms of $h(\mathbf{x}, t)$ and its associated conjugate response field $\hat{h}(\mathbf{x}, t)$ [27] that is formally equivalent to Eq. (1) together with the noise correlations in Eq. (2). Corrections to the parameters due to fluctuations are computed through one-loop Feynman diagrams (see the Supplemental Material (SM) [27]). At the one-loop order, the nonlinear couplings λ and λ_1 do not receive any relevant corrections. In contrast, ν acquires divergent corrections at one loop order. Dimensional analysis allows us to identify an effective dimensionless coupling constant g having $d_c = 4 + y$ and a dimensionless ratio γ defined as

$$g = k_d \frac{\lambda^2 D}{\nu^3}, \quad \gamma = \frac{\lambda_1}{\lambda}. \quad (4)$$

Using $d = 4 + y - \epsilon$ near d_c , the RG differential recursion relations ($\exp(l)$ is a dimensionless length) up to $\mathcal{O}(\epsilon)$ are

$$\frac{dD}{dl} = D[z + y - d - 2\chi], \quad (5)$$

$$\frac{d(\lambda, \lambda_1)}{dl} = (\lambda, \lambda_1)[\chi + z - 4], \quad (6)$$

$$\frac{d\nu}{dl} = \nu[z - 4 + g\Delta(\gamma, y)], \quad (7)$$

$$\frac{dg}{dl} = g[\epsilon - 3g\Delta(\gamma, y)], \quad (8)$$

together with $d\gamma/dl = d/dl(\lambda_1/\lambda) = 0$. Here,

$$\Delta \equiv \frac{1}{2(4+y)} \left[1 + \gamma(10 + 2y) + \gamma^2 \left(\frac{8y + 36}{6 + y} \right) \right]. \quad (9)$$

Furthermore, z and χ are the dynamic and roughness exponents, respectively [2]. See also [27]. At $d = d_c$, $\Delta(\gamma, y) > 0$ (violet region in Fig. 1(a)), $g = 0$ is the *only* fixed point (which is stable) of (8); but its approach to 0 is so slow that ν still gets *infinitely renormalized*, giving logarithmic modulations of the linear theory results $z = 4$ and $\chi = 0$. This is reminiscent of anomalous elasticity in three-dimensional equilibrium smectics [28, 29], 2D equilibrium elastic sheet having vanishing thermal expansion coupled with Ising spins [30, 31] and generalized quasi-long-range order in an active, diffusive XY model [32, 33].

Width $\mathcal{W} \equiv \langle [h(\mathbf{x}, t) - \bar{h}(t)]^2 \rangle^{1/2}$ grows initially with time and eventually saturates to a steady value $\mathcal{W}_{\text{sat}} \sim [\ln(L/a_0)]^{1/3}$. Here $\bar{h}(t)$ is the mean height at time t , L is the system size and a_0 a microscopic cutoff. In spite of the one-loop perturbative origin of this result, it is in fact *exact* in the asymptotic long wavelength limit. In the present theory, at the one-loop order $g(l) \sim 1/l$ for

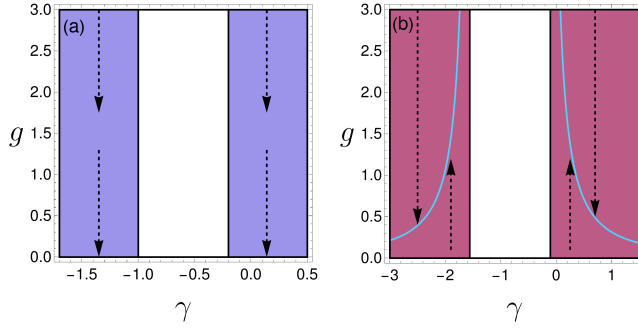


FIG. 2. ($\bar{\nu} = 0$). RG flow diagram in $d = 2$ for the (a) CKPZ+ model. The violet region is the perturbatively accessible logarithmic rough phase, while the central white region is unstable. In the accessible region, the RG flow lines (indicated by arrows) flow toward the stable fixed line $g = 0$. (b) MBE+ model. The blue line within the stable (red) region denotes the stable fixed line, toward which the RG flow lines converge.

large l in the stable, weak coupling phase. Higher-loop corrections should entail corrections to this $1/l$ -behavior, which vanish faster than $1/l$, giving finite corrections to ν . This leaves the scaling of \mathcal{W}_{sat} with L unchanged; see Refs. [17, 32, 33] for similar arguments. White region in Fig. 1(a) where $\Delta(\gamma, y) < 0$ is the strong-coupling regime speculated to be unstable. The above results hold so long as the “RG time” ℓ^* at which the nonlinearities become important is less than $\ln(\bar{\xi}/a_0)$, such that any substantial renormalization of ν can take already place. An estimation of ℓ^* can be made by setting $\nu \sim \Delta\nu(l)$, the one-loop correction to ν , giving $\ell^* \sim 1/[g_0\Delta(\gamma, y)]$, where g_0 is the “RG initial” value of g . We must also require $\bar{\xi} > a_0 \exp(\ell^*)$, else $\bar{\nu}\nabla^2h$ becomes dominant *before* the nonlinear effects becomes dominant.

To explore the unstable regime, we first consider the bare perturbation theory for ν , which is same as the RG calculations for ν except that now we extend the integrals over wave vectors down to an infrared cutoff $q_{\text{min}} = 2\pi/L$ with $L < \bar{\xi}$. Setting $d = d_c$, we get

$$\nu_{\text{eff}} \approx \nu_0 + g\nu_0\Delta(\gamma, y) \ln(L/a), \quad (10)$$

for the effective ν . Thus, for $\Delta(\gamma, y) < 0$, we have $\nu_{\text{eff}} < \nu_0$ for sufficiently large system sizes. This means variance of the local normal fluctuations $\langle(\delta\mathbf{n}^2)\rangle$ diverges for a sufficiently large size, where $\mathbf{n} \approx (1, -\nabla h) \equiv (1, \delta\mathbf{n})$ assuming small fluctuations. Thus the surface has only short range orientational order, a telltale signature of a crumpled surface. This strongly suggests that for parameters in the white region in Fig. 1(a), the surface is crumpled, a conclusion further supported by our MCT and numerical studies.

We now focus on $d < d_c$. Using the RG flow equations for $d < d_c$ ($\epsilon > 0$), when $\Delta(\gamma, y) > 0$, the plane $g^* = \epsilon/(3\Delta(\gamma, y))$ (blue plane in Fig. 1(b)) is a stable

fixed plane in the γ - y - g space, giving $z = 4 - \epsilon/3$ and $\chi = \epsilon/3$, while $g^* = 0$ is unstable. For $\Delta(\gamma, y) < 0$ (white region in Fig. 1(b)), $g^* = 0$ is the only fixed plane but unstable, indicating a strong-coupling (crumpled) phase [23]. For $d > d_c$ ($\epsilon < 0$) and $\Delta(\gamma, y) < 0$, $g^* = 0$ is a stable fixed plane spanned by γ - y - g with linear theory exponents $z = 4$, $\chi = -|\epsilon|/2$, while $g^* = |\epsilon|/(3|\Delta(\gamma, y)|)$ (blue plane in Fig. 1(c)) is unstable, signaling a roughening transition [2, 23]. For $\Delta(\gamma, y) > 0$ and $\epsilon < 0$, $g^* = 0$ remains the only stable plane, giving a smooth phase (green region in Fig. 1(c)). With $\epsilon < 0$, if $\Delta(\gamma, y) > (<)0$, $g(l)$ approaches (moves away from) the stable (unstable) fixed point $g^* = 0$ ($|\epsilon|/(3|\Delta(\gamma, y)|)$) of (8) *exponentially fast* (diverges at a finite RG scale l_c as $g(l_c) \sim \mathcal{O}(1)$, beyond which perturbative RG breaks down), thus identifying $d_c = 4 + y$ as the *upper (lower)* critical dimension. See also Refs. [17, 32, 33].

We briefly revisit the $d = 2$ cases: CKPZ+ ($y = -2$) and MBE+ ($y = 0$), studied in Refs. [22, 23]. For CKPZ+, with $d_c = 2$, bare perturbation theory predicts instability for $-1.0 < \gamma < -0.2$ [white region in Fig. 2(a)], while the stable phase (violet) shows linear exponents $z = 4$, $\chi = 0$, and logarithmic roughening. For MBE+ [Fig. 2(b)], the red region is stable with a fixed line $g^* = 2/(3\Delta(\gamma))$, with $\Delta(\gamma) = \frac{3}{4}\gamma^2 + \frac{5}{4}\gamma + \frac{1}{8}$, giving $z = 10/3$, $\chi = 2/3$, consistent with the LDS class [20]. The white region ($-1.559 < \gamma < -0.106$) is believed to be unstable or crumpled [23].

This instability can be cut off by the $\bar{\nu}\nabla^2h$ in (1) in the long wavelength limit, if the “RG time” l_c at which $g(l_c)$ becomes $\mathcal{O}(1)$ is substantially bigger than $\ln(\bar{\xi}/a_0)$. Setting $g(l_c) \sim 1$ gives another “correlation length” $\xi \sim a_0 \exp(l_c) \sim \exp[(1 - g_0)/3g_0|\Delta(\gamma, y)|]$. If $\bar{\xi} < \xi$, the long wavelength behavior is controlled by $\bar{\nu}$ and D , which due to the absence of any fluctuation-corrections for both $\bar{\nu}, D$ give $z = 2$ and $\chi = (2 + y - d)/2$, else for $\bar{\xi} > \xi$, the surface gets crumpled *before* the stabilizing $\bar{\nu}$ -term becomes important.

To further analyze the unstable regions observed in the RG flow diagrams, we now employ a one-loop MCT calculation [9, 16, 34–36] to extract the associated scaling behavior for $\bar{\nu} \approx 0$. In the present problem, due to the absence of any diverging correction to the noise amplitude (an *exact* statement) and the lack of relevant vertex corrections at the one-loop order, MCT entails only solving G self-consistently. The response function $G(\mathbf{k}, \omega)$ has the scaling form

$$G(\mathbf{k}, \omega) = k^{-z} g\left(\frac{\omega}{k^z}\right) = \frac{1}{-i\omega + \Sigma(\mathbf{k}, \omega)}, \quad (11)$$

where the self-energy $\Sigma(\mathbf{k}, \omega = 0) = \Gamma k^z$ in the zero frequency limit. The correlator is constructed in the Lorentzian approximation valid for low ω [18, 27].

By combining the contributions from all the relevant one-loop diagrams for $G^{-1}(\mathbf{k}, \omega = 0)$ and assuming the dominant contribution comes from the infra-red limit, we

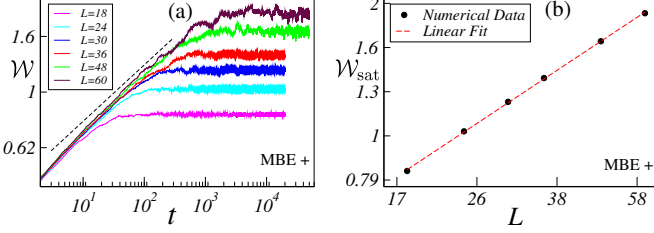


FIG. 3. For MBE+ model in $d = 2$, log-log plots (with $\bar{\nu} = 0, \nu = 1, D = 1, \nu_r = 0.2, \lambda = 2, \lambda_1 = 1$, and time step (δt) = 10^{-3}) of (a) W versus t . The black dashed line indicates a linear fit in the growth regime, yielding $\beta = 0.207 \pm 7.26 \times 10^{-5}$. (b) W_{sat} versus L . The red dashed line represent linear fit to the numerical data displayed on a log-log scale, with slope $\chi = 0.707 \pm 0.006$.

arrive at the dominant one-loop contribution to the self-energy [27] $k_d \frac{\lambda^2 D}{\Gamma^2} \tilde{\Delta}_m(\gamma, y, z) k^4 \frac{k^{4+d-y-2z}}{y+2z-4-d}$, where

$$\tilde{\Delta}_m(\gamma, y, z) = \left[\frac{2+y+z-d}{4d} + \gamma^2 \left(\frac{1}{d} + \frac{3(y+z)}{d(d+2)} \right) + \gamma \left(\frac{y+z+d-1}{2d} + \frac{3(2+y+z)}{2d(d+2)} \right) \right]. \quad (12)$$

assuming $\tilde{\Delta}_m(\gamma, y, z) > 0$ and $4+d-y-2z < 0$. With $\epsilon > 0$ ($d < d_c$) and $\tilde{\Delta}_m > 0$, matching k -powers with the bare term Γk^z yields $z = 4 - \epsilon/3$ and $\chi = \epsilon/3$ (using $\chi + z = 4$), consistent with RG. For $\tilde{\Delta}_m < 0$, MCT fails, indicating a crumpled phase. This is distinct from the MCT of KPZ equation see e.g., [9, 14–16, 37], in which MCT *does not* fail in the strong coupling phase. Thus, the strong coupling phases in (1) is clearly distinct from that in the KPZ equation. At $d = d_c$ we get $z = 4$, with one-loop correction to the self-energy [27], $k_d \frac{\lambda^2 D}{\Gamma^2} \ln(\Lambda/k) \Delta_m(\gamma, y)$, with

$$\Delta_m = \frac{1}{2(4+y)} \left[1 + \gamma(10 + 2y) + \gamma^2 \left(\frac{8y + 36}{6 + y} \right) \right]. \quad (13)$$

The obtained $\Delta_m(\gamma, y)$ exactly matches the RG result $\Delta(\gamma, y)$ in Eq. (9). The MCT approach breaks down for $\Delta(\gamma, y) < 0$, signaling an instability or crumpling of the surface. See Fig. 1(a) white region. This suggests that the model is no longer valid in this region. With $\Delta(\gamma, y) > 0$, the model remains stable, yielding the scaling exponents $z = 4$ and $\chi = 0$ in agreement with RG. For CKPZ+ model ($y = -2$) $d = d_c = 2$, MCT predicts the model is unstable in the range $-1.0 < \gamma < -0.2$, consistent with RG results [Fig. 2(a)]. For the MBE+ model ($y = 0$), MCT identifies an unstable window $-0.936 < \gamma < -0.254$. Outside this range, $z = 10/3$ and $\chi = 2/3$, in agreement with RG [Fig. 2(b)]. The slight mismatch between MCT and RG unstable regions arises from the ϵ -expansion used in RG. Independent of whether the surface remains stable or not for length scales

$< \xi$, with $\bar{\nu} < 0$ there is long wavelength instability that would dominate for a sufficiently large $L > \xi$.

To validate our results, we perform direct numerical simulations (DNS) for both CKPZ+ and MBE+ models at $d = 2$ with $\bar{\nu} = 0$. We include a regularizing term $\nu_r \nabla^6 h$, $\nu_r > 0$ in Eq. (1) to control numerical instabilities [22, 38–40]. The simulations are carried out using a pseudo-spectral method with the 2/3 dealiasing rule and an Euler scheme [41] for time integration. Fig. 3(a) shows W vs. t for the MBE+ model at $\gamma = 0.5$ (stable region of Fig. 2(b)) for different system sizes, averaged over several realizations, yielding $\beta = 0.207 \pm 7.26 \times 10^{-5}$. Fig. 3(b) display the variation of W_{sat} with L , respectively, giving $\chi = 0.707 \pm 0.006$. These results confirm algebraic scaling in the MBE+ model, in close agreement with RG predictions $\chi = 2/3$. Numerical results for CKPZ+ are known [22], with stable-region details given in SM [27]. To investigate the unstable regime, we fix $\delta t = 10^{-4}$, set $\lambda = 2$, and vary λ_1 to tune γ . The term $\nu_r \nabla^6 h$ stabilizes short-wavelength modes but is irrelevant in the unstable region $\nu < 0$. For $L > L_c \sim \sqrt{\nu_r/|\nu|} \approx 0.45$, height and normal fluctuations diverge, indicating possible membrane crumpling [42]. Figs. 4(a)[(b)] show $W(t)$ for CKPZ+ (MBE+) models with $L = 36$ [30] across several γ values in the unstable region of Fig. 2, where W diverges without saturation. Insets show γ values from the stable domains, where W saturates, confirming the

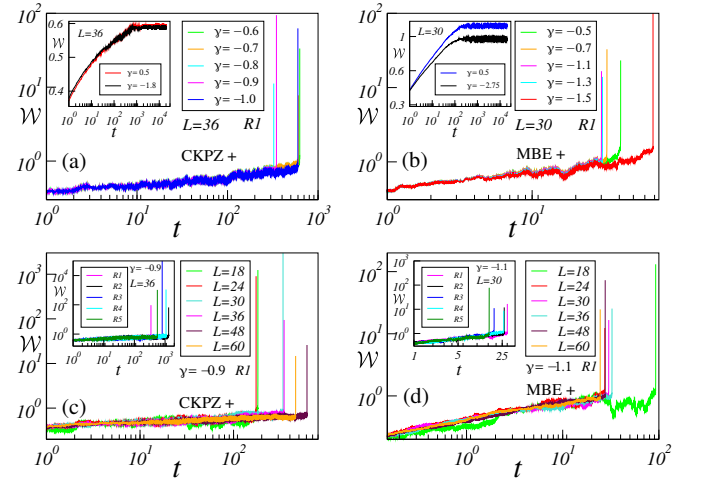


FIG. 4. Log-log plots of W versus t for various values of γ in the unstable region of Fig. 2, for a fixed realization ($R1$) and fixed L . Inset: log-log plots of W versus t for various values of γ in the stable region of Fig. 2, where W (averaged over many realizations) saturates, for the (a) CKPZ+ model (b) MBE+ model. Log-log plots of W versus t for various system sizes but fixed realization and fixed γ in the unstable region. Inset: same but for a fixed L , fixed γ , and over different realizations, for the (c) CKPZ+ model and (d) MBE+ model. Parameters $\bar{\nu} = 0, \nu = 1, D = 1, \nu_r = 0.2, \lambda = 2$, with various values of λ_1 (i.e., γ), and time step $\delta t = 10^{-3}$ (10^{-4}) in the stable (unstable) region.

white region as unstable. Figs. 4(c)[(d)] show $\mathcal{W}(t)$ for varying L at fixed γ in the unstable regime, with insets displaying different realizations for fixed L, γ for CKPZ+ (MBE+) models. The consistently diverging \mathcal{W} confirms our speculations that this region is unstable. This agrees with previous studies of the deterministic CKPZ+ equation in 2D, which reported blowup solutions for particular combinations of λ and λ_1 [43, 44].

To summarize, we have studied a generalized conserved surface growth model that in two distinct limits reduce to the CKPZ+ and MBE+ equations. We show that in the strong coupling phases of this equation, achieved for sufficiently strong nonlocal contributions to the chemical potential, the surface is unstable. We use a variety of techniques, analytical and numerical, to argue that this unstable surface is actually a crumpled surface. This makes the strong coupling phases in this model and the associated roughening transition distinct from those in the KPZ equations in $d > 2$. Nonrenormalization of λ in the present model holds only at the one-loop order [45]. While this can potentially make our results quantitatively inaccurate, our predictions on crumpling, corroborated by DNS studies, should generally hold. It will be interesting to study the spatio-temporal fluctuations of a conserved density on a conserved fluctuating surface as here [46–48] and the consequence of coupling of a conserved surface with an elastic network [49, 50], or with quenched disorder [51].

Acknowledgment:- The authors thank A. Haldar for various helpful suggestions. A.B. thanks the AvH Stiftung (Germany) for partial financial support under the Research Group Linkage Programme scheme (2024).

Kardar-Parisi-Zhang equation,” *Phys. Rev. E* **50**, 4560 (1994).

- [8] K. Moser, J. Kertész, and D. E. Wolf, “Numerical solution of the Kardar-Parisi-Zhang equation in one, two and three dimensions,” *Phys. A: Stat. Mech. Appl.* **178**, 215 (1991).
- [9] J. K. Bhattacharjee, “Upper critical dimension of the Kardar-Parisi-Zhang equation,” *J. Phys. A Math. Gen.* **31**, L93 (1998).
- [10] J. P. Bouchaud and M. E. Cates, “Self-consistent approach to the Kardar-Parisi-Zhang equation,” *Phys. Rev. E* **47**, R1455 (1993).
- [11] T. Hwa and E. Frey, “Exact scaling function of interface growth dynamics,” *Phys. Rev. A* **44**, R7873 (1991).
- [12] J. P. Doherty, M. A. Moore, J. M. Kim, and A. J. Bray, “Generalizations of the Kardar-Parisi-Zhang equation,” *Phys. Rev. Lett.* **72**, 2041 (1994).
- [13] Y. Tu, “Absence of finite upper critical dimension in the spherical Kardar-Parisi-Zhang model,” *Phys. Rev. Lett.* **73**, 3109 (1994).
- [14] J. K. Bhattacharjee and S. Bhattacharyya, *Nonlinear Dynamics Near and Far from Equilibrium* (Springer, New York, 2007).
- [15] A. Basu and E. Frey, “Novel universality classes of coupled driven diffusive systems,” *Phys. Rev. E* **69**, 015101 (R) (2004).
- [16] A. Basu and E. Frey, “Scaling and universality in coupled driven diffusive models,” *J. Stat. Mech.* **2009**, P08013 (2009).
- [17] D. Jana, A. Haldar, and A. Basu, “Logarithmic or algebraic: Roughening of an active Kardar-Parisi-Zhang surface,” *Phys. Rev. E* **109**, L032104 (2024).
- [18] D. Jana and A. Basu, “Rough or crumpled: Strong coupling phases of a generalized Kardar-Parisi-Zhang surface,” *Phys. Rev. E* **112**, L012104 (2025).
- [19] T. Sun, H. Guo, and M. Grant, “Dynamics of driven interfaces with a conservation law,” *Phys. Rev. A* **40**, 6763 (1989).
- [20] Z.-W. Lai and S. Das Sarma, “Kinetic growth with surface relaxation: Continuum versus atomistic models,” *Phys. Rev. Lett.* **66**, 2348 (1991).
- [21] J. Krug, “Origins of scale invariance in growth processes,” *Advances in Physics* **46**, 139 (1997).
- [22] F. Caballero, C. Nardini, F. van Wijland, and M. E. Cates, “Strong coupling in conserved surface roughening: A new universality class?” *Phys. Rev. Lett.* **121**, 020601 (2018).
- [23] S. Mukherjee and A. Basu, “Rough or crumpled: Phases in kinetic growth with surface relaxation,” *Phys. Rev. E* **106**, L022102 (2022).
- [24] D. Nelson, T. Piran, and S. Weinberg, *Statistical Mechanics of Membranes and Surfaces* (World Scientific, Singapore, 1989).
- [25] D. Forster, D. R. Nelson, and M. J. Stephen, “Large-distance and long-time properties of a randomly stirred fluid,” *Phys. Rev. A* **16**, 732 (1977).
- [26] P. C. Hohenberg and B. I. Halperin, “Theory of dynamic critical phenomena,” *Rev. Mod. Phys.* **49**, 435 (1977).
- [27] “See Supplemental Material for the one-loop Feynman diagrams used in the Renormalization Group analysis, details of the MCT calculations, and numerical method.”
- [28] G. Grinstein and R. A. Pelcovits, “Anharmonic Effects in Bulk Smectic Liquid Crystals and Other ”One-

* debayanjana96@gmail.com

† abhik.123@gmail.com, abhik.basu@saha.ac.in

- [1] M. Kardar, G. Parisi, and Y. C. Zhang, “Dynamic scaling of growing interfaces,” *Phys. Rev. Lett.* **56**, 889 (1986).
- [2] A-L Barabási and H. E. Stanley, *Fractal concepts in surface growth* (Cambridge University Press, Cambridge, 1995).
- [3] T. Halpin-Healy and Y. C. Zhang, “Kinetic roughening phenomena, stochastic growth, directed polymers and all that: aspects of multidisciplinary statistical mechanics,” *Physics Reports* **254**, 215 (1995).
- [4] L. Giada, A. Giacometti, and M. Rossi, “Pseudospectral method for the Kardar-Parisi-Zhang equation,” *Phys. Rev. E* **65**, 036134 (2002).
- [5] C. H. Lam and F. G. Shin, “Improved discretization of the Kardar-Parisi-Zhang equation,” *Phys. Rev. E* **58**, 5592 (1998).
- [6] R. Gallego, M. Castro, and J. M. López, “Pseudospectral versus finite-difference schemes in the numerical integration of stochastic models of surface growth,” *Phys. Rev. E* **76**, 051121 (2007).
- [7] M. Beccaria and G. Curci, “Numerical simulation of the

Dimensional Solids", " *Phys. Rev. Lett.* **47**, 856 (1981).

[29] G. Grinstein and R. A. Pelcovits, "Smectic- $A-C$ transition in three dimensions," *Phys. Rev. A* **26**, 2196 (1982).

[30] S. Mukherjee and A. Basu, "Stiffening or softening of elastic media: Anomalous elasticity near phase transitions," *Phys. Rev. E* **106**, L052102 (2022).

[31] S. Mukherjee and A. Basu, "Statistical mechanics of phase transitions in elastic media with vanishing thermal expansion," *Phys. Rev. E* **106**, 054128 (2022).

[32] A. Haldar, A. Sarkar, S. Chatterjee, and A. Basu, "Mobility-induced order in active XY spins on a substrate," *Phys. Rev. E* **108**, L032101 (2023).

[33] A. Haldar, A. Sarkar, S. Chatterjee, and A. Basu, "Active XY model on a substrate: Density fluctuations and phase ordering," *Phys. Rev. E* **108**, 034114 (2023).

[34] A. Kr. Chattopadhyay, A. Basu, and J. K. Bhattacharjee, "Coupled nonequilibrium growth equations: Self-consistent mode coupling using vertex renormalization," *Phys. Rev. E* **61**, 2086 (2000).

[35] A. Basu, "Statistical properties of driven magnetohydrodynamic turbulence in three dimensions: Novel universality," *Europhys. Lett.* **65**, 505 (2004).

[36] A. Basu and J. K. Bhattacharjee, "Universal properties of three-dimensional magnetohydrodynamic turbulence: Do Alfvén waves matter?" *J. Stat. Mech.* **2005**, P07002 (2005).

[37] T. Halpin-Healy, "Disorder-induced roughening of diverse manifolds," *Phys. Rev. A* **42**, 711 (1990).

[38] A. Basu, A. Sain, S. K. Dhar, and R. Pandit, "Multi-scaling in models of magnetohydrodynamic turbulence," *Phys. Rev. Lett.* **81**, 2687 (1998).

[39] S. S. Ray and A. Basu, "Universality of scaling and multi-scaling in turbulent symmetric binary fluids," *Phys. Rev. E* **84**, 036316 (2011).

[40] G. Sahoo, N. B. Padhan, A. Basu, and R. Pandit, "Direct Numerical Simulations of Three-dimensional Magnetohydrodynamic Turbulence with Random, Power-law Forcing," *arXiv:2011.04277* (2020).

[41] R. Mannella, *Stochastic Processes in Physics, Chemistry, and Biology* (Springer, New York, 2000) p. 353–364.

[42] S. Mukherjee and A. Basu, "Flat or crumpled: States of active symmetric membranes," *Phys. Rev. E* **112**, L013402 (2025).

[43] C. Escudero, "Geometric principles of surface growth," *Phys. Rev. Lett.* **101**, 196102 (2008).

[44] C. Escudero, F. Gazzola, and I. Peral, "Global existence versus blow-up results for a fourth order parabolic pde involving the hessian," *Journal de Mathématiques Pures et Appliquées* **103**, 924–957 (2015).

[45] H. K. Janssen, "On Critical Exponents and the Renormalization of the Coupling Constant in Growth Models with Surface Diffusion," *Phys. Rev. Lett.* **78**, 1082 (1997).

[46] T. Banerjee and A. Basu, "Symmetries and scaling in generalised coupled conserved Kardar-Parisi-Zhang equations," *Journal of Statistical Mechanics: Theory and Experiment* **2018**, 013202 (2018).

[47] S. Mukherjee, "Noise cross correlations can induce instabilities in coupled driven models," *Phys. Rev. E* **108**, 024219 (2023).

[48] S. Mukherjee, "Reduced fluctuations: Surprising effects of noise cross correlations in a coupled, driven model," *arXiv:2509.17763* (2025).

[49] T. Banerjee, N. Sarkar, J. Toner, and A. Basu, "Rolled Up or Crumpled: Phases of Asymmetric Tethered Membranes," *Phys. Rev. Lett.* **122**, 218002 (2019).

[50] T. Banerjee, N. Sarkar, J. Toner, and A. Basu, "Statistical mechanics of asymmetric tethered membranes: Spiral and crumpled phases," *Phys. Rev. E* **99**, 053004 (2019).

[51] S. Mukherjee, "Conserved Kardar-Parisi-Zhang equation: Role of quenched disorder in determining universality," *Phys. Rev. E* **103**, 042102 (2021).

[52] R. Bausch, H. K. Janssen, and H. Wagner, "Renormalized field theory of critical dynamics," *Z. Phys. B* **24**, 113 (1976).

[53] Uwe C Täuber, *Critical dynamics: a field theory approach to equilibrium and non-equilibrium scaling behavior* (Cambridge University Press, Cambridge, 2014).

[54] V. Yakhot and S. A. Orszag, "Renormalization group analysis of turbulence. I. Basic theory," *J. Sci. Comput.* **1**, 3 (1986).

Supplemental Material

RENORMALIZATION GROUP CALCULATIONS

We start by constructing a generating functional [52, 53] by using Eq. (1) and Eq. (2) of the main text. We get

$$\mathcal{Z} = \int \mathcal{D}\hat{h} \mathcal{D}h e^{-\mathcal{S}[\hat{h}, h]}, \quad (14)$$

where \hat{h} is referred as response field and \mathcal{S} is action functional, which is given by

$$\mathcal{S} = - \int_{\mathbf{k}, t} |\mathbf{k}|^{-y} D|\hat{h}|^2 + \int_{x, t} \hat{h}(\partial_t h - \bar{\nu}\nabla^2 h + \nu\nabla^4 h + \frac{\lambda}{2}\nabla^2(\nabla h)^2 + \lambda_1\nabla_i\nabla_j(\nabla_i h\nabla_j h)). \quad (15)$$

Results from the harmonic theory or the linearized equation of motion

This can be obtained from the Gaussian part of the action functional (15), i.e., by setting $\lambda = \lambda_1 = 0$ in (15). We first define Fourier transforms in space and time by

$$h(\mathbf{x}, t) = \int_{\mathbf{k}, \omega} h(\mathbf{k}, \omega) e^{i(\mathbf{k} \cdot \mathbf{x} - \omega t)}.$$

Then the (bare) two-point functions in the Gaussian limit of (15) are

$$\langle \hat{h}(\mathbf{k}, \omega) \hat{h}(-\mathbf{k}, -\omega) \rangle_0 = 0, \quad (16a)$$

$$\langle \hat{h}(\mathbf{k}, \omega) h(-\mathbf{k}, -\omega) \rangle_0 = \frac{1}{i\omega + \bar{\nu}k^2 + \nu k^4}, \quad (16b)$$

$$\langle \hat{h}(-\mathbf{k}, -\omega) h(\mathbf{k}, \omega) \rangle_0 = \frac{1}{-i\omega + \bar{\nu}k^2 + \nu k^4}, \quad (16c)$$

$$\langle h(\mathbf{k}, \omega) h(-\mathbf{k}, -\omega) \rangle_0 = \frac{2D|\mathbf{k}|^{-y}}{\omega^2 + (\bar{\nu}k^2 + \nu k^4)^2}. \quad (16d)$$

Fig. 5 shows the diagrammatic representations of the various two-point functions.

One-loop corrections to ν

We provide the details of the one-loop RG calculations for $\bar{\nu} = 0$. The one-loop Feynman diagrams, that contribute to the fluctuation correction of ν is shown in Fig. 6, for various vertex combinations. Figure 6(a) has a symmetry factor of 8. Its contribution is given by

$$\lambda^2 \int_{\mathbf{q}, \Omega} k^2 q_i (k - q)_i q^2 (q - k)_j k_j \times \frac{1}{-i\Omega + \nu q^4} \times \frac{2D|\mathbf{k} - \mathbf{q}|^{-y}}{\Omega^2 + \nu^2(k - q)^8}. \quad (17)$$

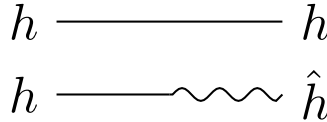


FIG. 5. Diagrammatic representations of two point functions.

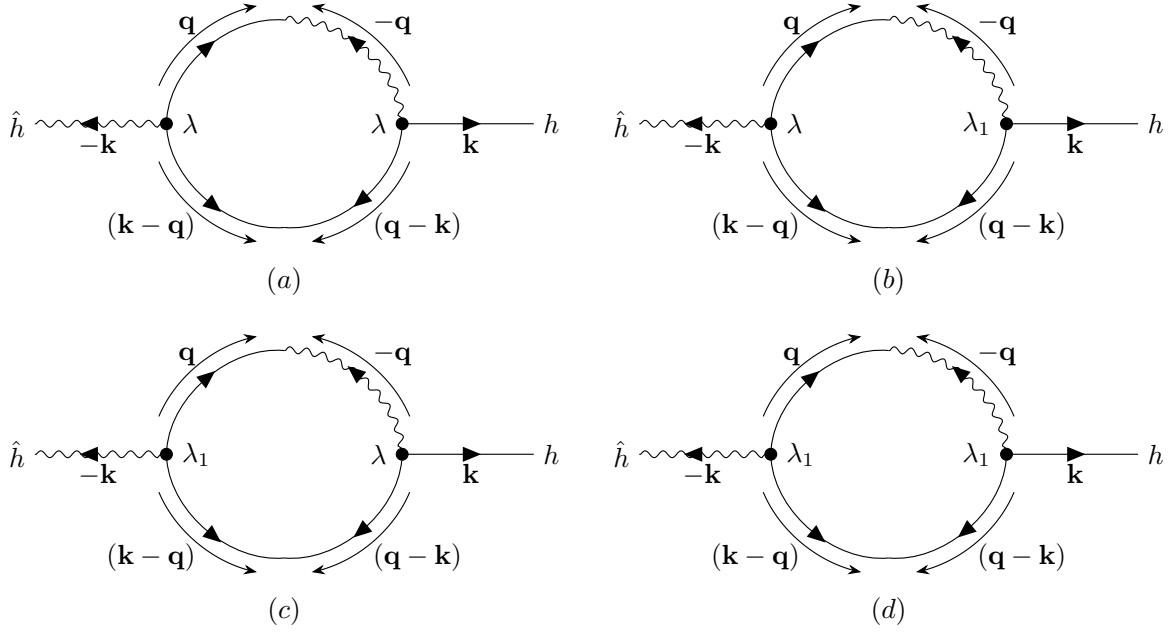


FIG. 6. One-loop Feynman diagrams that contribute to the renormalization of ν

After performing the Ω -integral and substituting

$$\int_{-\infty}^{\infty} \frac{d\Omega}{2\pi} \frac{1}{(-i\Omega + \nu q^4)(\Omega^2 + \nu^2(k-q)^8)} = \frac{1}{2\nu^2(k-q)^4[(k-q)^4 + q^4]}$$

in above equation, we obtain,

$$\frac{\lambda^2 D}{\nu^2} (k^2 k_j) \int_{\mathbf{q}} \frac{q_i (k-q)_i q^2 (q-k)_j}{|\mathbf{k} - \mathbf{q}|^{4+y} [(k-q)^4 + q^4]}. \quad (18)$$

After symmetrizing, i.e., making $\mathbf{q} \rightarrow \mathbf{q} + \mathbf{k}/2$, the numerator and denominator separately become

$$\begin{aligned} q_i (k-q)_i q^2 (q-k)_j &= -q^4 q_j + q^4 \frac{k_j}{2} - q^2 q_j q_m k_m, \\ \frac{1}{|\mathbf{k} - \mathbf{q}|^{4+y} [(k-q)^4 + q^4]} &= \frac{1}{2q^{8+y}} \left[1 + \left(\frac{4+y}{2} \right) \frac{\mathbf{k} \cdot \mathbf{q}}{q^2} \right]. \end{aligned}$$

Substituting these in Eq. (18) we obtain three integrals

$$\mathcal{I}_1 = \frac{\lambda^2 D}{\nu^2} (k^2 k_j) \int_{\mathbf{q}} \frac{-q^4 q_j \left(\frac{4+y}{2} \right) \frac{k_m q_m}{q^2}}{2q^{8+y}} = -\frac{\lambda^2 D}{\nu^2} \left(\frac{4+y}{4d} \right) k^4 \int \frac{d^d q}{q^{4+y}}, \quad (19)$$

$$\mathcal{I}_2 = \frac{\lambda^2 D}{\nu^2} (k^2 k_j) \int_{\mathbf{q}} \frac{q^4 k_j}{4q^{8+y}} = \frac{\lambda^2 D}{\nu^2} \frac{1}{4} k^4 \int \frac{d^d q}{q^{4+y}}, \quad (20)$$

$$\mathcal{I}_3 = \frac{\lambda^2 D}{\nu^2} (k^2 k_j) \int_{\mathbf{q}} \frac{-q^2 q_j q_m k_m}{2q^{8+y}} = -\frac{\lambda^2 D}{\nu^2} \frac{1}{2d} k^4 \int \frac{d^d q}{q^{4+y}}. \quad (21)$$

Here, $\mathcal{I}_1, \mathcal{I}_3$ is evaluated by using the well-known relation [54]

$$k_i k_j \int d^d q f(q^2) q_i q_j = k_i k_j \times \frac{[\delta_{ij}]}{d} \int d^d q f(q^2) q^2. \quad (22)$$

Adding above three integrals we obtain correction to ν from vertex ($\lambda-\lambda$) and it is

$$-\frac{\lambda^2 D}{\nu^2} k^4 k_d \left(\frac{6+y-d}{4d} \right) \int q^{d-y-5} dq. \quad (23)$$

Here $k_d = \frac{S_d}{(2\pi)^d}$, where S_d is the surface area of a d -dimensional unit sphere. Fig. 6(b) has a symmetry factor of 4. Its contribution is given by

$$2\lambda\lambda_1 \int_{\mathbf{q},\Omega} k^2 \mathbf{q} \cdot (\mathbf{k} - \mathbf{q}) q_i q_j k_i (q - k)_j \times \frac{1}{-i\Omega + \nu q^4} \times \frac{2D|\mathbf{k} - \mathbf{q}|^{-y}}{\Omega^2 + \nu^2(k - q)^8}, \quad (24)$$

$$= \frac{2\lambda\lambda_1 D}{\nu^2} (k^2 k_i) \int_{\mathbf{q}} \frac{q_m (k - q)_m q_i q_j (q - k)_j}{|\mathbf{k} - \mathbf{q}|^{4+y} [(k - q)^4 + q^4]}. \quad (25)$$

After symmetrization, i.e., making $\mathbf{q} \rightarrow \mathbf{q} + \mathbf{k}/2$, the above integral can be written as the sum of two separate integrals. These are

$$\mathcal{I}_4 = \frac{2\lambda\lambda_1 D}{\nu^2} (k^2 k_i) \int_{\mathbf{q}} \frac{-q^4 q_i \left(\frac{4+y}{2}\right) k_m q_m}{2q^{8+y}} = -\frac{2\lambda\lambda_1 D}{\nu^2} \left(\frac{4+y}{4d}\right) k^4 \int \frac{d^d q}{q^{4+y}}, \quad (26)$$

$$\mathcal{I}_5 = \frac{2\lambda\lambda_1 D}{\nu^2} (k^2 k_i) \int_{\mathbf{q}} \frac{-q^4 k_i}{4q^{8+y}} = -\frac{2\lambda\lambda_1 D}{\nu^2} \frac{1}{4} k^4 \int \frac{d^d q}{q^{4+y}}. \quad (27)$$

Similarly, Fig. 6(c) has a symmetry factor of 4 and its contribution is

$$2\lambda\lambda_1 \int_{\mathbf{q},\Omega} k_i k_j q_i (k - q)_j q^2 \mathbf{k} \cdot (\mathbf{q} - \mathbf{k}) \times \frac{1}{-i\Omega + \nu q^4} \times \frac{2D|\mathbf{k} - \mathbf{q}|^{-y}}{\Omega^2 + \nu^2(k - q)^8}, \quad (28)$$

$$= \frac{2\lambda\lambda_1 D}{\nu^2} (k_i k_j k_m) \int_{\mathbf{q}} \frac{q_i (k - q)_j q^2 (q - k)_m}{|\mathbf{k} - \mathbf{q}|^{4+y} [(k - q)^4 + q^4]}. \quad (29)$$

After symmetrization, i.e., making $\mathbf{q} \rightarrow \mathbf{q} + \mathbf{k}/2$, the above integral can be written as the sum of three separate integrals. These are

$$\mathcal{I}_6 = \frac{2\lambda\lambda_1 D}{\nu^2} (k_i k_j k_m) \int_{\mathbf{q}} \frac{-q_i q_j q^2 q_m \left(\frac{4+y}{2}\right) k_n q_n}{2q^{8+y}} = -\frac{2\lambda\lambda_1 D}{\nu^2} \frac{3}{d(d+2)} \left(\frac{4+y}{4}\right) k^4 \int \frac{d^d q}{q^{4+y}}, \quad (30)$$

$$\mathcal{I}_7 = \frac{2\lambda\lambda_1 D}{\nu^2} (k_i k_j k_m) \int_{\mathbf{q}} \frac{q_i q_j q^2 k_m}{4q^{8+y}} = \frac{2\lambda\lambda_1 D}{\nu^2} \frac{1}{4d} k^4 \int \frac{d^d q}{q^{4+y}}, \quad (31)$$

$$\mathcal{I}_8 = \frac{2\lambda\lambda_1 D}{\nu^2} (k_i k_j k_m) \int_{\mathbf{q}} \frac{-q_i q_j q_m q_n k_n}{2q^{8+y}} = -\frac{2\lambda\lambda_1 D}{\nu^2} \frac{3}{2d(d+2)} k^4 \int \frac{d^d q}{q^{4+y}}. \quad (32)$$

Here in evaluating \mathcal{I}_6 , \mathcal{I}_8 , we have used the following identity [54]

$$k_i k_j k_m k_n \int d^d q f(q^2) q_i q_j q_m q_n = k_i k_j k_m k_n \frac{[\delta_{ij}\delta_{mn} + \delta_{im}\delta_{jn} + \delta_{in}\delta_{jm}]}{d(d+2)} \int d^d q f(q^2) q^4. \quad (33)$$

Adding Eqs. (26), (27) and (30)-(32) we obtain correction to ν from vertex (λ - λ_1) and it is

$$-\frac{\lambda\lambda_1 D}{\nu^2} k^4 k_d \left(\frac{(3+d+y)}{2d} + \frac{3(6+y)}{2d(d+2)}\right) \int q^{d-y-5} dq. \quad (34)$$

Lastly, Fig. 6(d) has a symmetry factor of 8 and its contribution is

$$4\lambda_1^2 \int_{\mathbf{q},\Omega} k_i k_j q_i (k - q)_j q_m q_n k_m (q - k)_n \times \frac{1}{-i\Omega + \nu q^4} \times \frac{2D|\mathbf{k} - \mathbf{q}|^{-y}}{\Omega^2 + \nu^2(k - q)^8}, \quad (35)$$

$$= \frac{4\lambda_1^2 D}{\nu^2} (k_i k_j k_m) \int_{\mathbf{q}} \frac{q_i (k - q)_j q_m q_n (q - k)_n}{|\mathbf{k} - \mathbf{q}|^{4+y} [(k - q)^4 + q^4]}. \quad (36)$$

After symmetrization, i.e., $\mathbf{q} \rightarrow \mathbf{q} + \mathbf{k}/2$, the above integral reduces to two separate integrals, which are

$$\mathcal{I}_9 = \frac{4\lambda_1^2 D}{\nu^2} (k_i k_j k_m) \int_{\mathbf{q}} \frac{-q^2 q_i q_j q_m \left(\frac{4+y}{2}\right) k_n q_n}{2q^{8+y}} = -\frac{4\lambda_1^2 D}{\nu^2} \frac{3}{d(d+2)} \left(\frac{4+y}{4}\right) k^4 \int \frac{d^d q}{q^{4+y}}, \quad (37)$$

$$\mathcal{I}_{10} = \frac{4\lambda_1^2 D}{\nu^2} (k_i k_j k_m) \int_{\mathbf{q}} \frac{-q^2 q_i q_j k_m}{4q^{8+y}} = -\frac{4\lambda_1^2 D}{\nu^2} \frac{1}{4d} k^4 \int \frac{d^d q}{q^{4+y}}. \quad (38)$$

Adding Eqs. (37), (38) we obtain correction to ν from vertex $(\lambda_1 - \lambda_1)$ and it is

$$-\frac{\lambda_1^2 D}{\nu^2} k^4 k_d \left(\frac{3(4+y)}{d(d+2)} + \frac{1}{d} \right) \int q^{d-y-5} dq. \quad (39)$$

Collecting all the corrections to ν i.e., adding Eqs. (23), (34) and (39) we obtain total correction to ν

$$\nu^< = \nu \left[1 + \frac{\lambda^2 D}{\nu^3} k_d \left[\frac{6+y-d}{4d} + \gamma \left(\frac{3+d+y}{2d} + \frac{3(6+y)}{2d(d+2)} \right) + \gamma^2 \left(\frac{3(4+y)}{d(d+2)} + \frac{1}{d} \right) \right] \int_{\Lambda/b}^{\Lambda} q^{d-y-5} dq \right]. \quad (40)$$

Here, $\gamma = \frac{\lambda_1}{\lambda}$, as defined in the main text.

Nonrenormalization of λ and λ_1

Here, we show that at the one-loop order there are no relevant corrections to λ and λ_1 . Fig. 7(a) has a symmetry factor 24 and includes corrections to both λ and λ_1 . Contribution from this diagram is

$$\begin{aligned} & -12D\lambda\lambda_1^2(k^2 k_{1i} k_{2n}) \int_{\mathbf{q}, \Omega} \frac{q^6 q_i q_n |\mathbf{q}|^{-y}}{(\Omega - i\nu q^4)^2 (\Omega + i\nu q^4)^2} \\ & = -3D\lambda\lambda_1^2(k^2 k_{1i} k_{2n}) \int_{\mathbf{q}} \frac{q_i q_n |\mathbf{q}|^{-y}}{\nu^3 q^6}. \end{aligned} \quad (41)$$

Similarly, Fig. 7(b) has a symmetry factor 48 and contributes

$$\begin{aligned} & -24D\lambda\lambda_1^2(k^2 k_{1i} k_{2n}) \int_{\mathbf{q}, \Omega} \frac{q^6 q_i q_n |\mathbf{q}|^{-y}}{(\Omega - i\nu q^4)^3 (\Omega + i\nu q^4)} \\ & = 3D\lambda\lambda_1^2(k^2 k_{1i} k_{2n}) \int_{\mathbf{q}} \frac{q_i q_n |\mathbf{q}|^{-y}}{\nu^3 q^6}. \end{aligned} \quad (42)$$

Equations (41) and (42), when added, gives zero contribution to the corrections of λ and λ_1 .

RG recursion relations

In the above, we have integrated out the dynamical fields with wavevectors $|\mathbf{k}|$ in the range $(\Lambda/b \leq |\mathbf{k}| \leq \Lambda)$ in the action functional (15). Next, we rescale space, time and fields to raise the wavevector cutoff of $|\mathbf{k}|$ back to Λ . We

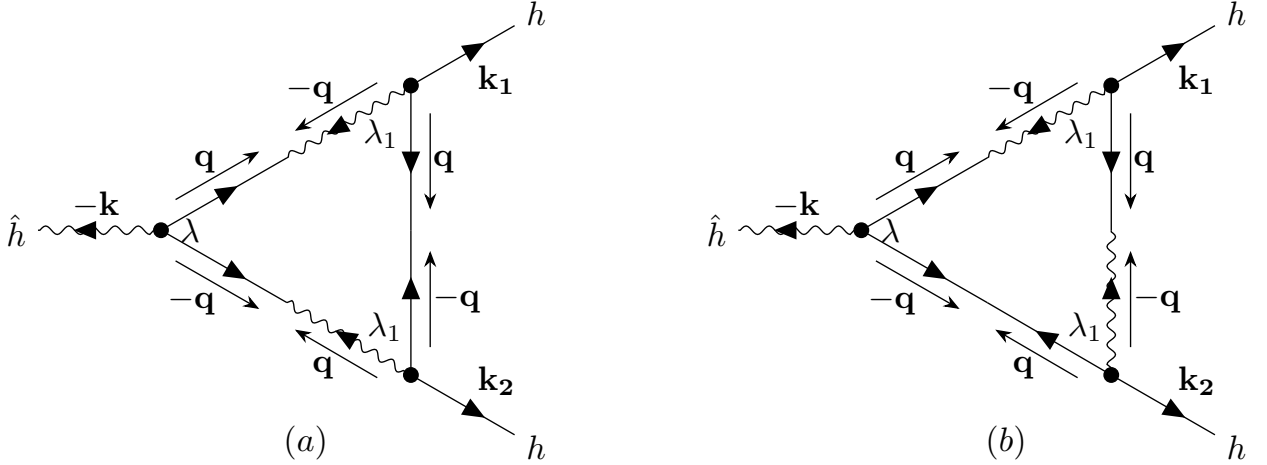


FIG. 7. One-loop Feynman diagrams giving the corrections to λ and λ_1 .

rescale $\mathbf{k} \rightarrow \mathbf{k}' = b\mathbf{k} \implies \mathbf{x} \rightarrow \mathbf{x}' = \frac{\mathbf{x}}{b}$ similarly, $\omega \rightarrow \omega' = b^z\omega \implies t' = \frac{t}{b^z}$. Furthermore, the fields are rescaled as

$$h^<(\mathbf{k}, \omega) = \xi h(\mathbf{k}', \omega'),$$

$$\hat{h}^<(\mathbf{k}, \omega) = \hat{\xi} \hat{h}(\mathbf{k}', \omega').$$

Using these we find that, model parameters scale as

$$\nu' = \nu^< b^{-d-4-z} \xi \hat{\xi},$$

$$D' = D^< b^{y-d-z} \hat{\xi}^2,$$

$$(\lambda', \lambda'_1) = (\lambda^<, \lambda_1^<) b^{-2d-4-2z} \hat{\xi} \xi^2.$$

Non-renormalization of D , λ , and λ_1 yields $(D^<, \lambda^<, \lambda_1^<) \equiv (D, \lambda, \lambda_1)$. Also, $h^<(\mathbf{x}, t)$ scale as $b^{-d-z} \xi h(\mathbf{x}', t')$. Defining $\xi_R = b^{-d-z} \xi = b^\chi$ and imposing the condition that coefficient of $\int_{\mathbf{x}, t} \hat{h} \partial_t h$ remains unity under rescaling, we get model parameters rescale as

$$\nu' = \nu^< b^{z-4},$$

$$D' = D b^{z+y-d-2\chi},$$

$$(\lambda', \lambda'_1) = (\lambda, \lambda_1) b^{\chi+z-4}.$$

Here, χ is the roughness exponent. Now we set $b = e^{\delta l} \approx 1 + \delta l$ for small δl , and define a dimensionless coupling constant by $g = k_d \frac{\lambda^2 D}{\nu^3}$ to obtain the flow equations

$$\frac{d\nu}{dl} = \nu \left[z - 4 + g \left[\frac{6+y-d}{4d} + \gamma \left(\frac{3+d+y}{2d} + \frac{3(6+y)}{2d(d+2)} \right) + \gamma^2 \left(\frac{3(4+y)}{d(d+2)} + \frac{1}{d} \right) \right] \right], \quad (43)$$

$$\frac{dD}{dl} = D(z+y-d-2\chi), \quad (44)$$

$$\frac{d(\lambda, \lambda_1)}{dl} = (\lambda, \lambda_1)(\chi+z-4), \quad (45)$$

$$\frac{dg}{dl} = g \left[4+y-d-3g \left[\frac{6+y-d}{4d} + \gamma \left(\frac{3+d+y}{2d} + \frac{3(6+y)}{2d(d+2)} \right) + \gamma^2 \left(\frac{3(4+y)}{d(d+2)} + \frac{1}{d} \right) \right] \right]. \quad (46)$$

See Eqs. (5)-(8) of the main text.

MCT CALCULATIONS

We start with the general definitions of the correlation function $C(\mathbf{k}, \omega)$ and response function $G(\mathbf{k}, \omega)$:

$$\delta^{(d)}(\mathbf{k} + \mathbf{k}') \delta(\omega + \omega') G(\mathbf{k}, \omega) = \left\langle \frac{\delta h(\mathbf{k}, \omega)}{\delta \eta(\mathbf{k}', \omega')} \right\rangle \quad (47)$$

$$\delta^{(d)}(\mathbf{k} + \mathbf{k}') \delta(\omega + \omega') C(\mathbf{k}, \omega) = \langle h(\mathbf{k}, \omega) h(\mathbf{k}', \omega') \rangle. \quad (48)$$

The response and correlation functions are assumed to have the following scaling form in the long time large length scale limit:

$$G(\mathbf{k}, \omega) = k^{-z} g\left(\frac{\omega}{k^z}\right) \quad (49)$$

$$C(\mathbf{k}, \omega) = k^{-y-2z} f\left(\frac{\omega}{k^z}\right), \quad (50)$$

where z is the dynamic exponent and χ is the roughness exponent; see also the main text for their definitions. The Dyson's equation for the self energy (Σ) is given by

$$G^{-1}(\mathbf{k}, \omega) = -i\omega + \Sigma(\mathbf{k}, \omega). \quad (51)$$

The zero frequency self energy or the relaxation rate has the form

$$\Sigma(\mathbf{k}, 0) = \Gamma k^z. \quad (52)$$

Here $\Gamma > 0$ is the effective damping coefficient. The correlation function in Lorentzian approximation can be written as

$$C(\mathbf{k}, \omega) = \frac{2D|\mathbf{k}|^{-y}}{\omega^2 + \Gamma^2 k^{2z}}, \quad (53)$$

giving the zero-frequency correlation function as

$$C(\mathbf{k}, 0) = \frac{2D}{\Gamma^2} |\mathbf{k}|^{-y-2z}. \quad (54)$$

Fig. 8(a) shows the one-loop diagrammatic correction to the self energy at $\mathcal{O}(\lambda^2)$ that comes with a symmetry factor

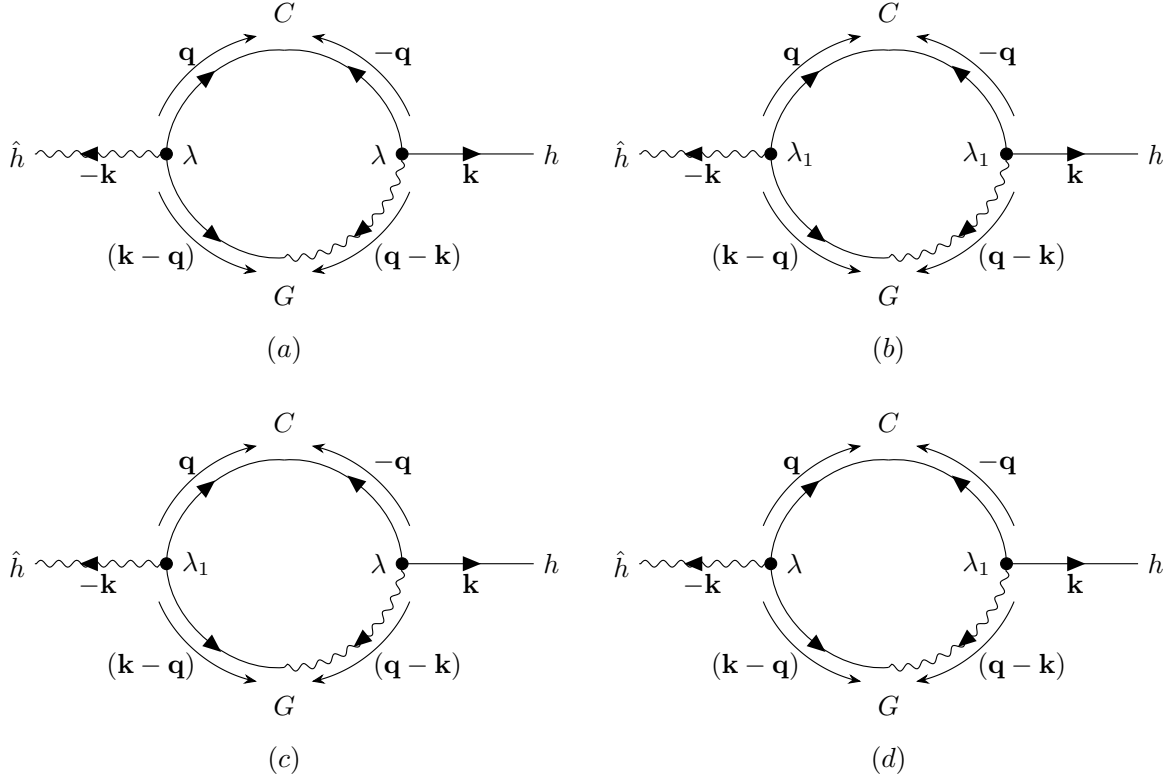


FIG. 8. One-loop Feynman diagrams that contribute to the zero frequency self energy in the MCT.

of 8 and contributes

$$\lambda^2 \int_{\mathbf{q}, \Omega} k^2 \mathbf{q} \cdot (\mathbf{k} - \mathbf{q}) (q - k)^2 (\mathbf{q} \cdot \mathbf{k}) C(\mathbf{q}, \Omega) G(\mathbf{k} - \mathbf{q}, -\Omega) = \lambda^2 k^2 k_i \int_{\mathbf{q}, \Omega} \frac{\mathbf{q} \cdot (\mathbf{k} - \mathbf{q}) (q - k)^2 q_i (2D) q^{-y}}{(\Omega^2 + \Gamma^2 q^{2z}) (i\Omega + \Gamma |\mathbf{k} - \mathbf{q}|^z)}. \quad (55)$$

After performing the Ω -integral, above integral becomes

$$\frac{\lambda^2 D}{\Gamma^2} k^2 k_i \int_{\mathbf{q}} \frac{q_j (k - q)_j (q - k)^2 q_i q^{-y-z}}{(q^z + |\mathbf{k} - \mathbf{q}|^z)}. \quad (56)$$

After symmetrization i.e. $\mathbf{q} \rightarrow \mathbf{q} + \frac{\mathbf{k}}{2}$, above integral simplifies to two integrals

$$\mathcal{I}_{11} = -k_d \frac{\lambda^2 D}{4\Gamma^2} k^4 \int_k^\Lambda q^{-y-2z+4+d-1} dq = -k_d \frac{\lambda^2 D}{4\Gamma^2} k^4 \left[\frac{k^{4+d-y-2z} - \Lambda^{4+d-y-2z}}{y+2z-4-d} \right], \quad (57)$$

$$\mathcal{I}_{12} = \frac{\lambda^2 D}{2\Gamma^2} k^2 k_i k_m (2+y+z) \int_{\mathbf{q}} \frac{q_i q_m}{2q^z} q^{-y-z+2} = k_d \frac{\lambda^2 D}{4\Gamma^2} \left(\frac{2+y+z}{d} \right) k^4 \left[\frac{k^{4+d-y-2z} - \Lambda^{4+d-y-2z}}{y+2z-4-d} \right]. \quad (58)$$

Adding the above contributions, we get the $\mathcal{O}(\lambda^2)$ correction to the zero frequency self energy

$$k_d \frac{\lambda^2 D}{4\Gamma^2} \left(\frac{2+y+z-d}{d} \right) k^4 \left[\frac{k^{4+d-y-2z} - \Lambda^{4+d-y-2z}}{y+2z-4-d} \right]. \quad (59)$$

Fig. 8(b) shows the one-loop contribution to the self energy at $\mathcal{O}(\lambda_1^2)$ with a symmetry factor of 8 and contributes

$$4\lambda_1^2 \int_{\mathbf{q},\Omega} k_i k_j q_i (k-q)_j (q-k)_m (q-k)_n q_m k_n \frac{2Dq^{-y}}{(\Omega^2 + \Gamma^2 q^{2z})(i\Omega + \Gamma |\mathbf{k} - \mathbf{q}|^z)}. \quad (60)$$

After performing the Ω -integral, we get

$$\frac{2D\lambda_1^2}{\Gamma^2} k_i k_j k_n \int_{\mathbf{q}} \frac{q_i (k-q)_j (q-k)_m (q-k)_n q_m q^{-y-z}}{q^z}. \quad (61)$$

Then shifting $\mathbf{q} \rightarrow \mathbf{q} + \frac{\mathbf{k}}{2}$ and extracting the $\mathcal{O}(k)$ contribution from the numerator, above integral reduces to two separate integrals

$$\mathcal{I}_{13} = \frac{2\lambda_1^2 D}{\Gamma^2} k_i k_j k_m k_n \left(\frac{y+z}{2} \right) \int_{\mathbf{q}} \frac{q_i q_j q_m q_n q^{-y-z}}{q^z} = k_d \frac{3\lambda_1^2 D}{\Gamma^2} \frac{(y+z)}{d(d+2)} k^4 \left[\frac{k^{4+d-y-2z} - \Lambda^{4+d-y-2z}}{y+2z-4-d} \right], \quad (62)$$

$$\mathcal{I}_{14} = \frac{\lambda_1^2 D}{\Gamma^2} k^2 k_i k_j \int_{\mathbf{q}} \frac{q_i q_j q^2 q^{-y-z}}{q^z} = k_d \frac{\lambda_1^2 D}{\Gamma^2} \frac{1}{d} k^4 \left[\frac{k^{4+d-y-2z} - \Lambda^{4+d-y-2z}}{y+2z-4-d} \right]. \quad (63)$$

Adding \mathcal{I}_{13} and \mathcal{I}_{14} we get contribution to zero frequency self energy at $\mathcal{O}(\lambda_1^2)$:

$$k_d \frac{\lambda_1^2 D}{\Gamma^2} \left(\frac{1}{d} + \frac{3(y+z)}{d(d+2)} \right) k^4 \left[\frac{k^{4+d-y-2z} - \Lambda^{4+d-y-2z}}{y+2z-4-d} \right]. \quad (64)$$

Fig. 8(c) gives one of the two one-loop corrections to the self energy at $\mathcal{O}(\lambda\lambda_1)$, with a symmetry factor of 4 and contributes

$$2\lambda\lambda_1 \int_{\mathbf{q},\Omega} k_i k_j q_i (k-q)_j (q-k)^2 (\mathbf{q} \cdot \mathbf{k}) \frac{2Dq^{-y}}{(\Omega^2 + \Gamma^2 q^{2z})(i\Omega + \Gamma |\mathbf{k} - \mathbf{q}|^z)}. \quad (65)$$

After performing the Ω -integral we get

$$\frac{\lambda\lambda_1 D}{\Gamma^2} k_i k_j k_m \int_{\mathbf{q}} \frac{q_i (k-q)_j (q-k)^2 q_m q^{-y-z}}{q^z}. \quad (66)$$

Again shifting $\mathbf{q} \rightarrow \mathbf{q} + \frac{\mathbf{k}}{2}$ and extracting the $\mathcal{O}(k)$ contribution from the numerator, above integral reduces to two separate integrals

$$\mathcal{I}_{15} = \frac{\lambda\lambda_1 D}{\Gamma^2} k_i k_j k_m k_n \int_{\mathbf{q}} \frac{q_i q_j q_m q_n q^{-y-z}}{q^z} = k_d \frac{\lambda\lambda_1 D}{\Gamma^2} \frac{3(2+y+z)}{2d(d+2)} k^4 \left[\frac{k^{4+d-y-2z} - \Lambda^{4+d-y-2z}}{y+2z-4-d} \right], \quad (67)$$

$$\mathcal{I}_{16} = -\frac{\lambda\lambda_1 D}{2\Gamma^2} k_i k_j k^2 \int_{\mathbf{q}} \frac{q_i q_j q^{-y-z+2}}{q^z} = -k_d \frac{\lambda\lambda_1 D}{2\Gamma^2} \frac{1}{d} k^4 \left[\frac{k^{4+d-y-2z} - \Lambda^{4+d-y-2z}}{y+2z-4-d} \right]. \quad (68)$$

Finally, Fig. 8(d) gives the second one-loop correction to the self energy that is also $\mathcal{O}(\lambda\lambda_1)$, but is distinct from the one in Fig. 8(c):

$$2\lambda\lambda_1 k^2 k_j \int_{\mathbf{q},\Omega} q_m (k-q)_m (q-k)_i (q-k)_j q_i \frac{2Dq^{-y}}{(\Omega^2 + \Gamma^2 q^{2z})(i\Omega + \Gamma |\mathbf{k} - \mathbf{q}|^z)}. \quad (69)$$

After performing the Ω -integral, above integral becomes

$$\frac{D\lambda\lambda_1}{\Gamma^2} k^2 k_j \int_{\mathbf{q}} \frac{q_m (k-q)_m (q-k)_i (q-k)_j q_i q^{-y-z}}{q^z}. \quad (70)$$

After shifting $\mathbf{q} \rightarrow \mathbf{q} + \frac{\mathbf{k}}{2}$, above integral reduces to two integrals

$$\mathcal{I}_{17} = \frac{\lambda\lambda_1 D}{\Gamma^2} \left(\frac{y+z}{2} \right) k^2 k_j k_m \int_{\mathbf{q}} \frac{q_j q_m q^{2-y-z}}{q^z} = k_d \frac{\lambda\lambda_1 D}{\Gamma^2} \frac{(y+z)}{2d} k^4 \left[\frac{k^{4+d-y-2z} - \Lambda^{4+d-y-2z}}{y+2z-4-d} \right], \quad (71)$$

$$\mathcal{I}_{18} = \frac{\lambda\lambda_1 D}{2\Gamma^2} k^4 \int_{\mathbf{q}} \frac{q^{4-y-z}}{q^z} = k_d \frac{\lambda\lambda_1 D}{2\Gamma^2} k^4 \left[\frac{k^{4+d-y-2z} - \Lambda^{4+d-y-2z}}{y+2z-4-d} \right]. \quad (72)$$

Adding integrals (\mathcal{I}_{15}) - (\mathcal{I}_{18}) we get the total $\mathcal{O}(\lambda\lambda_1)$ contribution to self energy at zero-frequency

$$k_d \frac{\lambda\lambda_1 D}{\Gamma^2} \left(\frac{y+z+d-1}{2d} + \frac{3(2+y+z)}{2d(d+2)} \right) k^4 \left[\frac{k^{4+d-y-2z} - \Lambda^{4+d-y-2z}}{y+2z-4-d} \right]. \quad (73)$$

Adding Eqs. (59), (64) and (73) we obtain total contribution to zero frequency self energy,

$$\begin{aligned} & k_d \frac{\lambda^2 D}{\Gamma^2} \left[\frac{2+y+z-d}{4d} + \gamma \left(\frac{y+z+d-1}{2d} + \frac{3(2+y+z)}{2d(d+2)} \right) + \gamma^2 \left(\frac{1}{d} + \frac{3(y+z)}{d(d+2)} \right) \right] k^4 \left[\frac{k^{4+d-y-2z} - \Lambda^{4+d-y-2z}}{y+2z-4-d} \right], \\ & = k_d \frac{\lambda^2 D}{\Gamma^2} \tilde{\Delta}_m(\gamma, y, z) k^4 \left[\frac{k^{4+d-y-2z} - \Lambda^{4+d-y-2z}}{y+2z-4-d} \right] \end{aligned}$$

Here,

$$\tilde{\Delta}_m(\gamma, y, z) = \left[\frac{2+y+z-d}{4d} + \gamma \left(\frac{y+z+d-1}{2d} + \frac{3(2+y+z)}{2d(d+2)} \right) + \gamma^2 \left(\frac{1}{d} + \frac{3(y+z)}{d(d+2)} \right) \right]. \quad (74)$$

At the critical dimension obtained from the RG analysis, i.e., $d = d_c = 4 + y$, equating the powers of k in the above expression with Γk^z yields the dynamic exponent $z = 4$. Substituting $z = 4$ in above expression we obtain correction to self energy at critical dimension,

$$\begin{aligned} & k_d \frac{\lambda^2 D}{\Gamma^2} \ln(\Lambda/k) \frac{1}{2(4+y)} \left[1 + \gamma(10+2y) + \gamma^2 \left(\frac{8y+36}{6+y} \right) \right], \\ & = k_d \frac{\lambda^2 D}{\Gamma^2} \ln(\Lambda/k) \Delta_m(\gamma, y). \end{aligned} \quad (75)$$

Here,

$$\Delta_m(\gamma, y) = \frac{1}{2(4+y)} \left[1 + \gamma(10+2y) + \gamma^2 \left(\frac{8y+36}{6+y} \right) \right]. \quad (76)$$

as given in the main text.

NUMERICAL DETAILS

To suppress numerical instabilities, we incorporate a higher-order regularization term $\nu_r \nabla^6 h$ ($\nu_r > 0$) into Eq. (1) of the main text. The evolution equation for the height field then reads

$$\partial_t h = \bar{\nu} \nabla^2 h - \nu \nabla^4 h - \frac{\lambda}{2} \nabla^2 (\nabla h)^2 - \lambda_1 \nabla_i \nabla_j (\nabla_i h \nabla_j h) + \nu_r \nabla^6 h + \eta. \quad (77)$$

We follow Ref. [22] and employ a pseudo-spectral method with the 2/3 dealiasing rule, combined with an Euler time-integration scheme [41], to simulate both MBE+ and CKPZ+ models in $d = 2$. Unless stated otherwise, the parameters are fixed at $\bar{\nu} = 0, \nu = 1, D = 1, \lambda = 2$, and $\nu_r = 0.2$. Simulations are performed on a square lattice with unit lattice spacing $a_0 = 1$.

We first focus on the stable regime. For $\lambda_1 = 1$, corresponding to $\gamma = 0.5$, which lies in the stable region of Fig. 2 of the main text, simulations are run up to total time $T = 20000$ for system sizes $L \leq 36$ and up to $T = 50000$ for larger systems ($L > 36$), using a time step $\delta t = 10^{-3}$. Fig. 9(a) shows the temporal evolution of the surface width $\mathcal{W}(t)$ for various L , averaged over R realizations ($R = 1000$ for $L = 18$ and $R = 50$ for $L = 60$). The width saturates after a finite time, as expected. Fig. 9(b) presents the scaling of the saturated width \mathcal{W}_{sat} with $\ln L$ on a log-log plot.

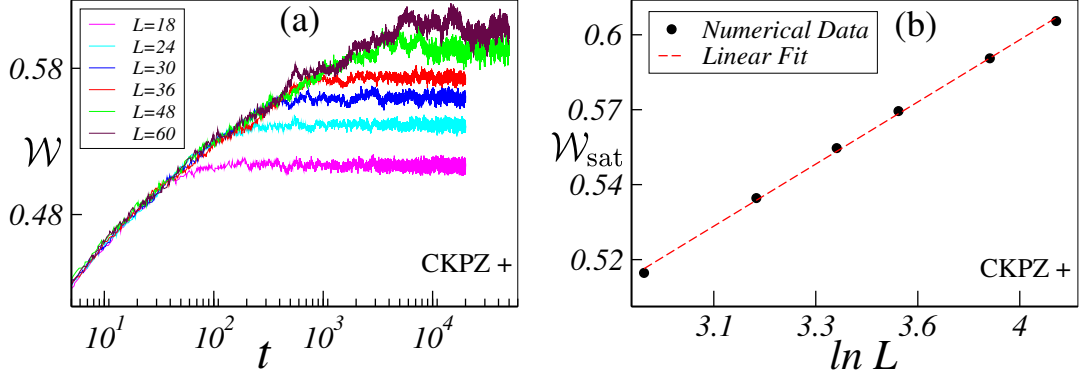


FIG. 9. Log-log plots of (a) width (W) versus time (t) for the CKPZ+ model for different system sizes. Width saturates in the stable region. (b) W_{sat} versus $\ln L$ for the CKPZ+ model. The red dashed line represent linear fit to the numerical data displayed on a log-log scale, showing logarithmic scaling behavior. These results are obtained for parameters $\bar{\nu} = 0, \nu = 1, D = 1, \nu_r = 0.2, \lambda = 2, \lambda_1 = 1$, and time step (δt) = 10^{-3} .

The data exhibit clear logarithmic scaling, consistent with theoretical predictions. Results for the MBE+ model are discussed in the main text.

To explore the dynamics in the unstable regime, we fix the time step at $\delta t = 10^{-4}$ and set $\lambda = 2$, while varying λ_1 to tune the parameter γ . The corresponding results are presented in the main text. These results consistently reveal a rapidly diverging surface width in the unstable sector, corroborating the RG and MCT predictions that this regime is intrinsically unstable and requires the inclusion of higher-order terms in Eq. (1) for stabilization.

For completeness, we summarize below the numerical protocol used in the simulations:

- **Integration scheme:** Pseudo-spectral method with the 2/3 dealiasing rule.
- **Time stepping:** Explicit Euler scheme [41].
- **Fixed parameters:** $\bar{\nu} = 0, \nu = 1, D = 1, \lambda = 2$, and $\nu_r = 0.2$.
- **Lattice:** Square grid with unit spacing $a_0 = 1$.
- **Simulation time:** $T = 20000$ for $L \leq 36$, and $T = 50000$ for $L > 36$ in stable region.
- **Time step:** $\delta t = 10^{-3}$ (10^{-4}) in the stable (unstable) regime.